Since January 2020 Elsevier has created a COVID-19 resource centre with free information in English and Mandarin on the novel coronavirus COVID-19. The COVID-19 resource centre is hosted on Elsevier Connect, the company's public news and information website.

Science of the Total Environment 754 (2021) 142226

Contents lists available at ScienceDirect

Science of the Total Environment

journal homepage: www.elsevier.com/locate/scitotenv

Impact of the COVID-19 outbreak on air pollution levels in East Asia

Masoud Ghahremanloo, Yannic Lops, Yunsoo Choi *, Seyedali Mousavinezhad

Department of Earth and Atmospheric Sciences, University of Houston, Houston, TX 77004, USA

HIGHLIGHTS

- Remote sensing data, TROPOMI and AHI were used to quantify lockdown impact.
- NO_2 experienced the highest decrease in East Asia due to lockdowns.
- NO_2 (83%) and SO_2 (71%) decreased more than HCHO (11%) and CO (4%) in Wuhan.
- SO_2 increased in Seoul and Tokyo due to polluted air transport in 2020.
- HCHO to NO_2 ratio increased from below 1 to above 2 in East China in February 2020.

GRAPHICAL ABSTRACT

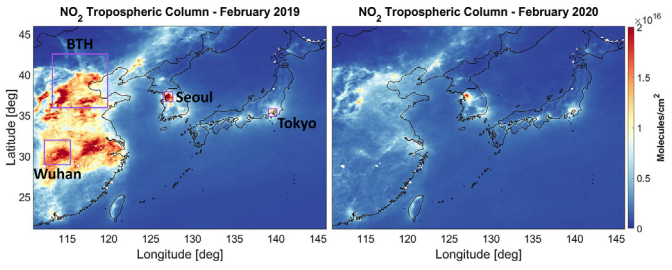

Region	BTH	Wuhan	Seoul	Tokyo
NO_2 percent change (2020-2019)	-53.71	-82.55	-33.05	-19.23

ARTICLE INFO

Article history:
Received 19 June 2020
Received in revised form 13 August 2020
Accepted 3 September 2020
Available online 7 September 2020

Editor: Jianmin Chen

Keywords:
Remote sensing
COVID-19
Air pollution
AOD
TROPOMI
Himawari-8
East Asia

ABSTRACT

This study leverages satellite remote sensing to investigate the impact of the coronavirus outbreak and the resulting lockdown of public venues on air pollution levels in East Asia. We analyze data from the Sentinel-5P and the Himawari-8 satellites to examine concentrations of NO_2, HCHO, SO_2, and CO, and the aerosol optical depth (AOD) over the BTH, Wuhan, Seoul, and Tokyo regions in February 2019 and February 2020. Results show that most of the concentrations of pollutants are lower than those of February 2019. Compared to other pollutants, NO_2 experienced the most significant reductions by almost 54%, 83%, 33%, and 19% decrease in BTH, Wuhan, Seoul, and Tokyo, respectively. The greatest reductions in pollutants occurred in Wuhan, with a decrease of almost 83%, 11%, 71%, and 4% in the column densities of NO_2, HCHO, SO_2, and CO, respectively, and a decrease of about 62% in the AOD. Although NO_2, CO, and formaldehyde concentrations decreased in the Seoul and Tokyo metropolitan areas compared to the previous year, concentrations of SO_2 showed an increase in these two regions due to the effect of transport from polluted upwind regions. We also show that meteorological factors were not the main reason for the dramatic reductions of pollutants in the atmosphere. Moreover, an investigation of the HCHO/NO_2 ratio shows that in many regions of East China, particularly in Wuhan, ozone production in February 2020 is less NO_X saturated during the daytime than it was in February 2019. With large reductions in the concentrations of NO_2 during lockdown situations, we find that significant increases in surface ozone in East China from February 2019 to February 2020 are likely the result of less reaction of NO and O_3 caused by significantly reduced NO_X concentrations and less NO_X saturation in East China during the daytime.

1. Introduction

Severe acute respiratory syndrome coronavirus 2 (SARS-CoV-2) is classified as a member of the order Nidovirales and part of the Coronaviridae family of viruses (Richman et al., 2016). Stemming from this family of viruses is coronavirus disease 2019 (COVID-19), first

* Corresponding author.
E-mail addresses: mghahremanloo@uh.edu (M. Ghahremanloo), ylops@central.uh.edu (Y. Lops), ychoi6@uh.edu (Y. Choi), smousavinezhad@uh.edu (S. Mousavinezhad).

https://doi.org/10.1016/j.scitotenv.2020.142226
0048-9697/

reported to the World Health Organization (WHO) in December 2019 (https://www.who.int/emergencies/diseases/novel-coronavirus-2019/events-as-they-happen; last access: 5 May 2020) with the first cases occurring in the city of Wuhan in Hubei Province, China. With the spread of the COVID-19, countries throughout the globe have issued lockdowns to combat the spread of the virus. Since the incipient state of the disease, the lockdowns have affected both people and industries during the epidemic and reduced concentrations of pollutants in the atmosphere by a significant amount (Wang et al., 2020). Regarding this, it is of great importance to investigate the impact of the COVID-19 outbreak and subsequent lockdown situations on atmospheric constituents to achieve a better understanding of the effects of the pandemic on the atmosphere.

The major criteria pollutants in the atmosphere are sulfur dioxide (SO_2), carbon monoxide (CO), nitrogen oxides (NO_X), particulate matter (PM), ozone (O_3), and volatile organic compounds (VOCs) (Zhang et al., 2016). Since human activity is one of the main sources releasing these major criteria pollutants into the atmosphere, it is expected that lockdown situations decrease concentrations of these pollutants in the atmosphere. NO_X is produced from the combustion of fossil fuels (Choi et al., 2009), biomass burning (van der Werf et al., 2006), soil microbial activity (Yienger and Levy, 1995), and lightning (Choi et al., 2009). These species react with VOCs in the presence of sunlight to form ground-level ozone. Chinese VOC and CO source contributions originate from vehicle emissions (Wu et al., 2017), biofuel and biomass burning, and industrial emissions (Guo et al., 2004). The majority of SO_2 emission sources within China are power plants (Lu et al., 2010); fortunately, with the implementation of environmental regulations, SO_2 emissions have steadily decreased (van der A et al., 2017). Both SO_2 and CO are primary gas-phase pollutants (Chen et al., 2001), and emission intensities have revealed their relationship to transition economies (Viguier, 1999).

It is estimated that China contributes 33, 24, 31, 21, and 20% of the global emissions of SO_2, NO_X, CO, Ammonia (NH_3), and Methane (CH_4), respectively (Hoesly et al., 2018). Most of these pollutants are precursors to PM and ozone, which exert harmful effects on human health (Nuvolone et al., 2018) and agriculture (Ainsworth, 2017). Studies have found that factors related to pollutants depend on meteorological and climatological factors such as winter haze (Mao et al., 2019), as well as PM_{10} and $PM_{2.5}$ (particulate matter with an aerodynamic diameter of <10 μm and 2.5 μm, respectively) pollution (Baltaci et al., 2020; Song et al., 2017). In addition, analyses of meteorological pollution have shown minor changes in anthropogenic emissions over extended periods of time. Despite the reduction of emissions (Richter et al., 2005; Zheng et al., 2018) and high pollution days (Li et al., 2019), the atmospheric chemistry of some regions of China has not improved, owing to unfavorable meteorological conditions (Yang et al., 2016) and dust transport (Baltaci, 2017; Yu et al., 2019). Hence, meteorological conditions also need to be considered due to their significance (Mehdipour and Memarianfard, 2017) in atmospheric constituents. The relationship between pollutants and the meteorological factors should be carefully investigated to draw a solid conclusion regarding the impact of less human activities on a decrease of pollutant levels in the atmosphere.

Health risk assessments have shown that short-term exposure to pollutants (e.g., ozone and particulate matter with an aerodynamic diameter of <10 μm (PM_{10})) is linked to respiratory and cardiovascular diseases (Mulenga and Siziya, 2019) that lead to increased hospital admissions and mortalities (Brunekreef and Holgate, 2002). On average, cardiorespiratory diseases accounted for 49% of non-accidental deaths within Chinese cities, and PM_{10} concentrations were significantly associated with these mortalities (Chen et al., 2011; Chen et al., 2012). It is estimated that at least 50,000 people in China die from chronic obstructive pulmonary disease (COPD) resulting from ozone concentrations that exceed safe levels and exposure time (Liu et al., 2018). The major ozone precursors responsible for these deaths are VOCs, NO_x, and CO (Placet et al., 2000); thus, reducing these precursors is critical to reducing tropospheric ozone levels. While PM concentrations originate from direct PM emissions, some PM concentrations originate from emission precursors (e.g., SO_2, VOCs, NO_x, and NH_3) through secondary formation within the atmosphere (Hodan and Barnard, 2004). Considering this, although COVID-19 is responsible for many deaths throughout the world, lockdown situations resulting from this pandemic can indirectly save lives through the decrease of pollutants from the atmosphere.

On January 23, 2020, Wuhan and several other cities within the Hubei Province were placed on lockdown, with Beijing and surrounding cities imposing travel restrictions the following day (WHO Timeline, 2020). On March 3, Japan closed primary and secondary schools, limited the hours of operation of many businesses, and supported stay-at-home work (Rush, 2020). At the same time, although a comprehensive restriction order was not imposed within Seoul, the government announced a voluntary stay-at-home advisory for the area at the end of February (Kim and Denyer, 2020; Normile et al., 2020). The effects of the mandatory shutdown of a large portion of the Chinese industry have provided a unique opportunity to analyze atmospheric changes that coincide with reductions in emissions and pollutants.

The last several decades have witnessed considerable advancements in the development of remote sensing applications in assessing, forecasting, and managing air quality (Mhawish et al., 2018). More specifically, satellite remote sensing instruments have provided valuable data on the global distribution of pollutants (Gupta et al., 2006; Martin, 2008; Lee et al., 2015), their evolution in time within the atmosphere (Zhang et al., 2012), and long-range transport (Kim et al., 2017; Wu et al., 2018). Such instruments measure specific features within the surface over an unprecedented program study period such as the Landsat program (Ghahremanloo et al., 2019; Loveland and Dwyer, 2012) or cover a vast amount of data products for diverse research applications such as the moderate resolution imaging spectroradiometer (MODIS) satellite program (Masuoka et al., 1998). For instance, remote sensing data enable the identification of NO_x-sensitive or NO_x-saturated regimes (Choi, 2013) and constrain NO_X emissions by NO_2 column remote sensing observations (Martin et al., 2003). Remote sensing tools provide the capability to measure emissions and pollution where in situ measurement systems are not readily available (Benaissa et al., 2019).

Geostationary remote sensing satellites such as the Advanced Himawari Imager (AHI) have dramatically improved the number of bands, spatial resolutions, and temporal frequencies and thus provide a diverse set of data products from the surface (e.g., sea surface temperature and vegetation) and atmospheric features (e.g., aerosols and stratospheric ozone) in a specific region (Bessho et al., 2016; Kramar et al., 2016; Zhang et al., 2019). Moreover, TROPOspheric Monitoring Instrument (TROPOMI) has been developed and deployed on the Copernicus Sentinel-5 Precursor satellite in 2017. TROPOMI, with a sun-synchronous orbit, measures global key atmospheric pollutants (Veefkind et al., 2012) at significantly improved spatio-temporal resolutions (Köhler et al., 2018). The combination of such diverse remote sensing satellites enables comprehensive remote sensing data validation, application, and analyses (de Laat et al., 2019; Lee et al., 2020).

The findings of significant changes in emissions provide researchers with a unique opportunity to analyze emission and pollutant transport within East Asia. In this study, we have leveraged the capability of satellite remote sensing to investigate the impact of the COVID-19 outbreak and subsequent lockdowns on declining pollutant levels in East Asia. This is the first comprehensive study investigating the impact of the COVID-19 lockdown situations on AOD and also concentrations of NO_2, HCHO, SO_2, CO, and ozone in BTH, Wuhan, Seoul, and Tokyo regions. In the following sections of the study, we first talk about the study area, data, and instruments that were used in this research. Then, we compare concentrations of atmospheric constituents to

measure the effects and significance of the pandemic, both spatially and in near real-time, of the previous year and during the initial outbreak of the virus. We also analyze the impact of drastic changes in anthropogenic emissions and meteorology to the significance of the change of atmospheric constituents due to the lockdown. In addition, we analyze the reasons for the significant increase in constituents despite the decrease in emissions during the lockdown period.

2. Methodology

We analyzed pollutant concentrations over East Asia (21° to 46° N and 111° to 146° E), including specific regions and cities such as the Beijing-Tianjin-Hebei (BTH) region, the Wuhan area, the Seoul metropolitan area (SMA), and the Tokyo metropolitan area (TMA). The BTH (36.05° to 42.66° N and 113.45° to 119.83° E), including the municipalities of Beijing and Tianjin and another 11 cities in the Hebei Province is a heavily industrialized area and one of the most polluted regions in China (Zhang et al., 2017; Zhao et al., 2018). To investigate the effects of the COVID-19 outbreak in metropolitan areas close to China, we selected a 3° × 3° area around the Wuhan city center and a 1° × 1° area around the SMA and the TMA. See the study area in Fig. 1.

In this study, we used satellite remote sensing data to analyze four major pollutants and the AOD, measured at 500 nm (nm), to investigate the intensity of emission reductions resulting from the lockdowns enforced by officials during the COVID-19 outbreak. We analyzed concentrations of nitrogen dioxide (NO_2), formaldehyde (HCHO), sulfur dioxide (SO_2), and carbon monoxide (CO) and used NO_2 and SO_2 as proxies for $PM_{2.5}$. We also investigated ozone production efficiency (OPE) and created a distribution map of the formaldehyde to nitrogen dioxide ratio (FNR) over the study area to investigate the chemical sensitivity of ozone production (OP) to its precursors over East Asia, and analyzed the impact of the lockdown on the chemical sensitivity of OP. We acquired the tropospheric column density of NO_2 and formaldehyde, along with total column densities of SO_2 and CO, from the TROPOspheric Monitoring Instrument (TROPOMI) onboard the Copernicus Sentinel-5 Precursor (Sentinel-5P) satellite and gathered 106 swath images of TROPOMI for February 2019 and February 2020 (henceforth referred to as 2019 and 2020). Before August 6, 2019, the spatial resolution of the TROPOMI images was 7 × 3.5 km for NO_2, formaldehyde and SO_2, and 7 × 7 km for CO. After this time, the spatial resolution was updated to 5.5 × 3.5 km and 5.5 × 7 km, respectively. To address the difference, all of the images from 2019 and 2020 were resampled at a resolution of 7 × 3.5 km for NO_2, formaldehyde, and SO_2 and 7 × 7 km for CO. We used all the swath images with a temporal resolution of 101.5 min over the study area to create daily images for the two months. In addition, we obtained daily AOD images for 2019 and 2020 from the Advanced Himawari Imager (AHI) onboard the Himawari-8 satellite, a geostationary satellite over East Asia at longitude 140.7° East. In total, we analyzed 56 daily AOD images with the spatial resolution of 5 × 5 km and obtained daily surface ozone concentrations for the two time periods from 1428 ground stations listed on China's Ministry of Ecology and Environment (MEE) public website (http://beijingair.sinaapp.com; last access: 5 May 2020).

We downloaded daily meteorological data from the Global Land Data Assimilation System (GLDAS) (https://ldas.gsfc.nasa.gov/gldas; last access: 5 May 2020) and the Modern-Era Retrospective analysis for Research and Applications, Version 2 (MERRA-2) (https://gmao.gsfc.nasa.gov/reanalysis/MERRA-2; last access: 5 May 2020) for 2019 and 2020. We obtained parameters, including air temperature (referred to in this study as "temperature"), specific humidity (referred to as "humidity"), and surface pressure (referred to as "pressure"), with the spatial resolution of 0.25 × 0.25°, from GLDAS and eastward and northward components of wind speed, with the spatial resolution of 0.5 × 0.625°, from MERRA-2. Then we performed comparative analyses of the four pollutants, the AOD, and meteorological parameters for 2019 and 2020 over the study area and matched pixels from satellite images to the GLDAS grid cells nearest to their centroids. Fig. S1 shows the flowchart representing the research methodology and Table 1 shows the list of acronyms used in this study.

3. Results and discussion

3.1. Aerosol optical depth (AOD)

The AOD is a measure of the extinction of electromagnetic radiation at a specific wavelength owing to the presence of particles such as pollutants, dust, and smoke in the atmospheric column (Chudnovsky et al., 2014). Since pollutants in the atmosphere absorb and scatter sunlight, reductions in the pollutant levels are expected to reduce AOD. It should be noted that pollutants are not the only factors altering AOD. Other elements (e.g., sea salt, dust) also influence the AOD value. Therefore, these factors can influence the direct relationship between air pollutant concentrations and AOD levels. We used the BSC-DREAM8b model, operated by the Barcelona Supercomputing Center (http://www.bsc.es/ess/bsc-dust-daily-forecast/; last access: 2 August 2020) to remove dusty days from February 2019 and February 2020. This way, we eliminated the major effects of dust on AOD levels in the study area. Fig. 2 shows the distribution of the AOD over the study area in 2019 and 2020. Major decreases in AOD values are observed in regions most impacted by the COVID-19 outbreak. The monthly AOD decreased by nearly 31% and 62% (see Table 2) in the BTH and Wuhan, respectively, from 2019 to 2020. Moreover, there were major reductions in the standard deviation of AOD levels within the BTH and especially Wuhan in 2020. The differences between maximum and minimum values of AOD levels within these two regions decreased, resulting in more homogeneous AOD levels within BTH and especially Wuhan. The AOD in the TMA, however, did not change dramatically since this metropolitan area was not under major lockdown conditions in February 2020.

Unlike BTH and Wuhan regions, the SMA experienced an increase in AOD levels. We attribute this increase to the significantly higher AOD levels in upwind regions of the SMA in 2020 than in 2019. High AOD levels in upwind regions of the SMA were likely due to the frequent dust storms in the eastern part of the Gobi Desert, located in regions northwest of the SMA. Although we removed the days with major transport of dust from desert regions, there is usually a consistent transport of dust to the upwind regions of SMA, making AOD levels of these regions higher than other neighboring areas. Regarding this, the effects of wind transport played an important role in the higher AOD levels of SMA in 2020. Wind patterns in the study area (Fig. S3) show that north-westerly winds were the main wind patterns affecting the SMA in 2020. In addition, the area was not as significantly affected by the COVID-19 outbreak and thus had less stringent lockdown situations than BTH and Wuhan. Because of the relatively high frequency of missing values in the daily AOD images, this study did not analyze the relationships between the AOD and meteorological factors. Table S1 displays the correlation between each pixel showing changes in AOD concentrations from 2019 to 2020 and its corresponding pixel showing changes in the meteorological patterns from 2019 to 2020 over the four regions. According to this table, only the AOD of the BTH region was influenced by temperature changes, while the other three regions showed no association with the meteorological factors. To validate this assumption, however, one should investigate the relationship of daily AOD levels to daily meteorological factors in greater detail.

3.2. Nitrogen dioxide (NO_2)

NO_2 primarily enters the atmosphere from both the burning of fossil fuels and the photochemical oxidation of nitric oxide emitted from combustion processes, soils, plants, and so on (Choi et al., 2009; Jacobson, 2005). Sunlight breaks the NO_2 down during the morning, which explains the lower concentrations of NO_2 during the midday or

Fig. 1. Map of East Asia, representing the study area. The black box (36.05° to 42.66° N and 113.45° to 119.83° E) represents the Beijing-Tianjin-Hebei (BTH) area in China, and purple dots represent Wuhan, Seoul, and Tokyo.

afternoon (Jacobson, 2005; Reed et al., 2016; Trebs et al., 2009). The lockdown provided conditions suitable for the atmosphere and sunlight to reduce NO_2 levels in East Asia. While the NO_2 column obtained from satellite images (see Fig. 4) showed dramatic reductions in NO_2 concentrations over the study area, especially in Wuhan and BTH, where concentrations of NO_2 declined nearly 54% and 83%, respectively, it showed only a moderate reduction of about 33% and 19% in the SMA and the TMA, respectively (see Table 3 for details). The extent of the reductions in NO_2 levels in these four regions is consistent with the severity of the COVID-19 outbreak and lockdown situations within these areas. It is worth noting that South Korea and Japan, like many other countries, enforced strict surveillance measures at airports, seaports, and border crossings to prevent the spread of COVID-19 into their countries. Management strategies that reduced travel (e.g., restricting air travel and enforcing airport lockdowns) contributed to the fewer infections and fewer lockdowns. Highly stringent lockdowns represent a significant determinant of major reductions in NO_2 concentrations in BTH and Wuhan. Wuhan was the most impacted region in East Asia, which experienced the most stringent lockdown situations compared to other regions of the study area. In this regard, the most reductions of the NO_2 concentrations happened in this region. Moreover, according to Table 3 and Fig. 4, the standard deviation of NO_2 concentrations in East China, especially in Wuhan, has decreased significantly, indicating that all areas within the Wuhan region have experienced a relatively clean atmosphere compared to February 2019. Other studies also reported significant reductions in NO_2 concentrations in Wuhan and different regions of the world, due to the COVID-19 outbreak and its resulting lockdown situations. According to Zambrano-Monserrate et al. (2020), NO_2 was decreased by 22.8 μg/m^3 and 12.9 μg/m^3 in Wuhan and China, respectively, due to the quarantine. They also reported dramatic reductions of NO_2 over Rome, Madrid, and Paris, the first cities in Europe to enforce strict quarantine measures. Moreover, Otmani et al. (2020) found a dramatic decrease of NO_2 in Salé, Morocco, where NO_2 concentrations decreased by 96% percent during the COVID-19 lockdown period compared to the days before the lockdown.

Fig. 3 displays the NO_2 daily trends in the four regions over the study area. The trends of daily averages show significant reductions in the concentration levels of NO_2 in BTH and especially in Wuhan. Regarding the SMA, the first few days saw no major reductions in the daily averaged NO_2 concentrations from the previous year. Major differences, however, appeared during the last 15 days of February, indicating a delay in the COVID-19 outbreak in the SMA (from that in BTH and Wuhan) and subsequent stay-at-home strategies. In the second half of February, with a stronger COVID-19 outbreak in South Korea, fewer activities took place in the SMA, resulting in fewer emissions of NO_2. Among the four regions investigated in this study, the TMA experienced the lowest reduction in NO_2 from 2019 to 2020. This is consistent with the extent of the COVID-19 outbreak and its resulting stay-at-home strategies in the four regions of the study area.

Table 4 shows relatively high correlations between daily NO_2 concentrations and daily temperature, pressure, and humidity in the four regions in 2019, but most of the correlations have decreased in

Table 1
List of acronyms.

AHI	Advanced Himawari Imager
AOD	Aerosol Optical Depth
BTH	Beijing-Tianjin-Hebei
CMAQ	Community Multiscale Air Quality
COPD	Chronic Obstructive Pulmonary Disease
COVID-19	COronaVIrus Disease of 2019
FNR	Formaldehyde to Nitrogen dioxide Ratio
GLDAS	Global Land Data Assimilation System
MEE	Ministry of Ecology and Environment
MERRA-2	Modern-Era Retrospective analysis for Research and Applications, Version 2
MODIS	MODerate resolution Imaging Spectroradiometer
OP	Ozone Production
OPE	Ozone Production Efficiency
PM	Particulate Matter
PM_{10}	Particulate Matter with an aerodynamic diameter of <10 μm
$PM_{2.5}$	Particulate Matter with an aerodynamic diameter of <2.5 μm
Sentinel-5P	Sentinel-5 Precursor
SMA	Soul Metropolitan Area
TMA	Tokyo Metropolitan Area
TROPOMI	TROPOspheric Monitoring Instrument
VOC	Volatile Organic Compound
WHO	World Health Organization

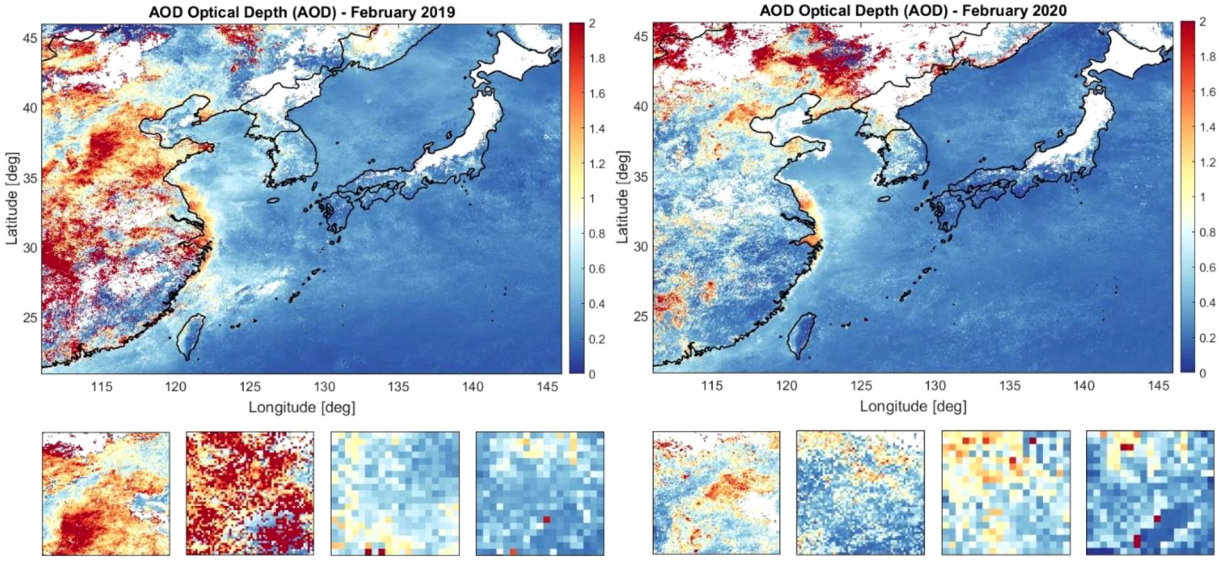

Fig. 2. Map of East Asia showing the aerosol optical depth (AOD) averaged over February 2019 and February 2020 over the study area. (a), (b), (c), and (d) refer to BTH, Wuhan, SMA, and TMA regions, respectively. The aerosol optical depth (AOD) is unitless.

2020, indicating that lockdowns were the main factor responsible for the decrease in NO_2 levels. For example, while the daily temperature and daily NO_2 concentrations in Wuhan were strongly correlated in 2019, their correlation was nearly zero in 2020. In 2020, the temperature in Wuhan was much higher than it was in 2019, but it showed no significant changes in other regions (see Table 4 and Fig. S4). Normally, as temperature increases, concentrations of H_2O increase, which results in increased OH concentrations. The increased OH partly expedites the formation of nitric acid from NO_2 and OH, which reduces the lifetime of NO_2. Moreover, an increase in the temperature can promote the upward motion of the air (Yang et al., 2017), which leads to more efficient diffusion conditions and decreases NO_2 levels. The slight correlation between daily temperature and daily NO_2 levels in Wuhan indicates that meteorological factors had very little impact on reducing the NO_2 levels of Wuhan in 2020.

Table 2
Mean, standard deviation, maximum, and minimum values of the aerosol optical depth (AOD) calculated during February 2019 and February 2020 over the BTH, Wuhan, SMA, and TMA regions. The AOD is unitless.

	BTH		Wuhan		Seoul		Tokyo	
	2019	2020	2019	2020	2019	2020	2019	2020
Mean	1.26	0.87	1.63	0.62	0.68	0.76	0.48	0.49
Std. deviation	0.54	0.40	0.84	0.33	0.24	0.31	0.22	0.37
Max value	4.99	4.71	4.99	2.8	2.51	2.06	1.89	4.3
Min value	0.01	0.09	0.03	0.1	0.3	0.19	0.17	0.01
Percent change	−30.9		−62.2		+12.46		+1.38	

3.3. Formaldehyde (HCHO)

Formaldehyde is released into the atmosphere by both anthropogenic and natural sources. Anthropogenic formaldehyde sources are mostly vehicle exhaust/emissions, different stationary combustion sources, and industrial emissions while natural sources include live and decaying plants, biomass burning, and other organic matters (Luecken et al., 2012; Pan et al., 2015; Shim et al., 2005). Responses to the COVID-19 outbreak influenced tropospheric concentrations of formaldehyde. As shown in Table 5, formaldehyde levels in East Asia decreased by 13% in BTH, 10% in Wuhan, 22% in the SMA, and 8% in the TMA. Table 4 also shows that the temperature in Wuhan increased by about 5° from February 2019 to February 2020. Temperature increase leads to increases in the number of biogenic emissions and oxidation processes to form formaldehyde from anthropogenic emissions of VOCs, which could explain the less dramatic decrease in formaldehyde levels in Wuhan after the lockdown. Because of the relatively high frequency of missing values in the daily measurements of the tropospheric column of formaldehyde within the four regions of the study area, we did not analyze the daily trends of formaldehyde together with their corresponding relationships with daily meteorological factors. Fig. 5, which represents the distribution of the tropospheric column density of formaldehyde over the study area, depicts noticeable reductions in the tropospheric column density of formaldehyde over the regions of the study area from 2019 to 2020. Table S2 displays the correlation between each pixel showing the changes in formaldehyde concentrations from 2019 to 2020 and its corresponding pixel showing changes in the meteorological patterns from 2019 to 2020 over the four regions. The table shows no significant

Table 3
Mean, the standard deviation, maximum and minimum values of the tropospheric column density of nitrogen dioxide (NO_2) calculated during February 2019 and February 2020 over the BTH, Wuhan, SMA, and TMA regions. All units for the mean, max, and min values are in molecules/cm^2.

	BTH		Wuhan		SMA		TMA	
	2019	2020	2019	2020	2019	2020	2019	2020
Mean	9.3E+15	4.3E+15	1.5E+16	2.5E+15	1.6E+16	1E+16	9.8E+15	7.9E+15
Std. deviation	6E+15	2.2E+15	3.4E+15	7.2E+14	5E+15	3.7E+15	2.1E+15	2.4E+15
Max value	4.1E+16	1.4E+16	3E+16	7.2E+15	3.1E+16	2.1E+16	1.5E+16	1.5E+16
Min value	2.3E+14	5.2E+14	7.2E+15	1.4E+15	5.1E+15	3.4E+15	5.3E+15	3.5E+15
Percent change	−53.71		−82.55		−33.05		−19.23	

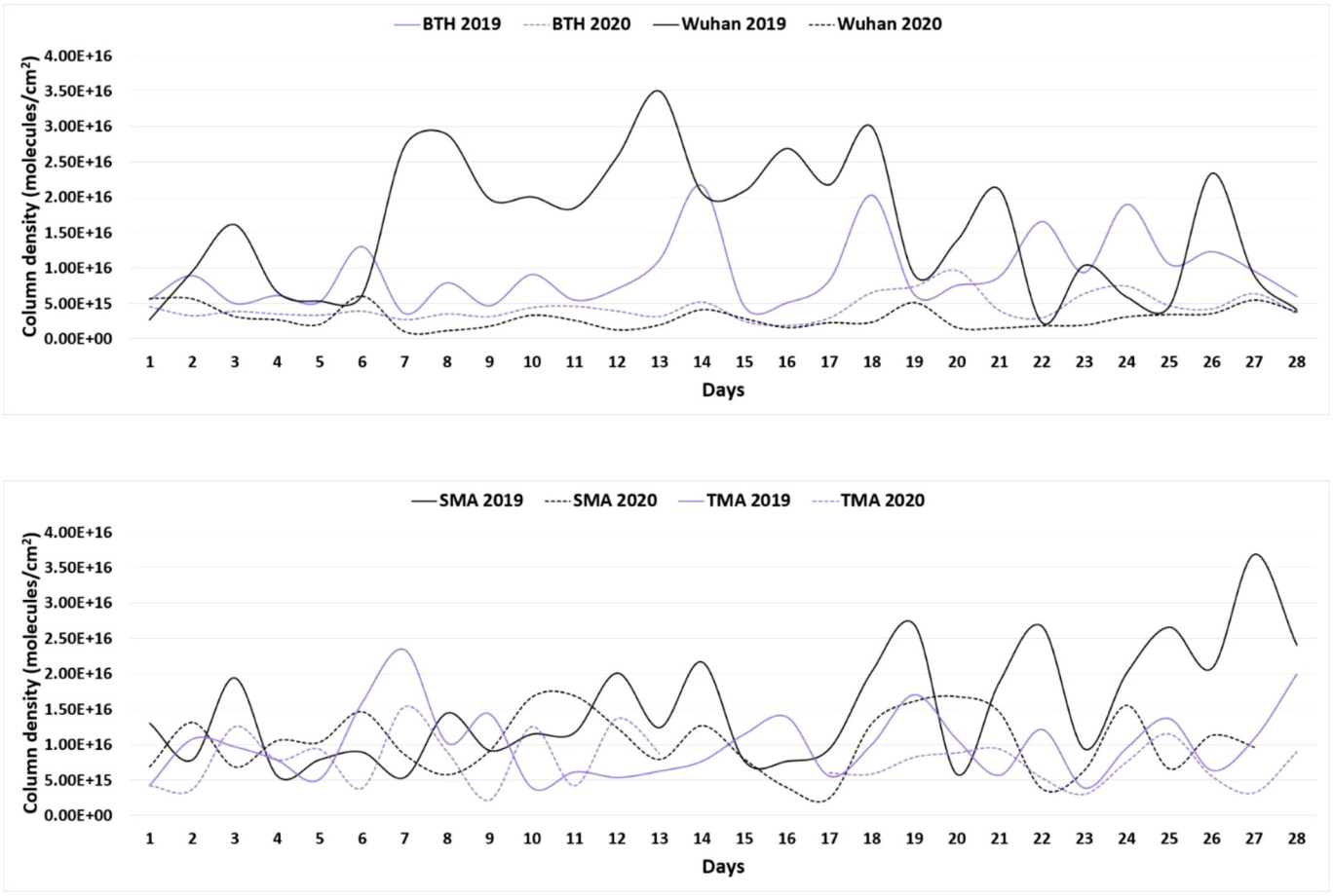

Fig. 3. Trend lines for the daily average of the tropospheric column density of nitrogen dioxide (NO_2) over the BTH, Wuhan, SMA, and TMA regions in February 2019 and February 2020. All units are in molecules/cm^2.

correlations between formaldehyde levels (2020–2019) and changes in the meteorological factors (2020–2019) within the four regions of the study area. One explanation for these low correlations is that meteorological factors such as temperature and anthropogenic sources of formaldehyde counteract one another and affect formaldehyde concentrations through a series of conflicting processes. For example,

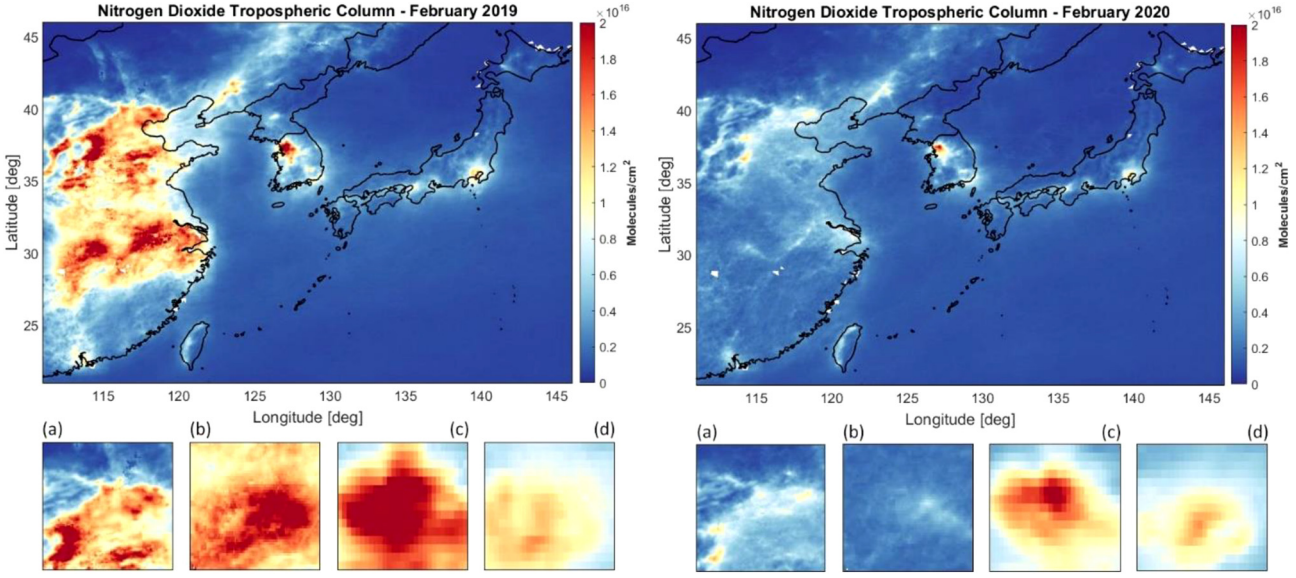

Fig. 4. Map of East Asia showing the average tropospheric column density of nitrogen dioxide (NO_2) in February 2019 and February 2020 over the study area. (a), (b), (c), and (d) refer to the BTH, Wuhan, SMA, and TMA regions, respectively. All units of the tropospheric column density of nitrogen dioxide (NO_2) are in molecules/cm^2.

Table 4
Monthly mean values for air temperature, surface pressure, and specific humidity calculated during February 2019 and February 2020 over the BTH, Wuhan, SMA, and TMA regions. The abbreviations Cor., Temp, Press, and Hum refer to correlation, air temperature (k), surface pressure (hPa), and specific humidity (kg/kg), respectively.

	BTH		Wuhan		SMA		TMA	
	2019	2020	2019	2020	2019	2020	2019	2020
Temp	270.3	272.5	277.9	283.2	274.2	275.2	281.2	282.1
Cor. temp & NO_2	0.23	0.43	−0.70	−0.05	0.50	0.32	0.27	0.14
Press	955.9	955.2	1010.1	1009.8	1012.2	1011.5	1013.0	1013.2
Cor. press & NO_2	−0.07	−0.14	0.52	−0.23	−0.21	0.41	−0.61	0.07
Hum	0.0014	0.0022	0.0040	0.0056	0.0018	0.0028	0.0034	0.0035
Cor. hum & NO_2	0.38	0.41	−0.42	0.05	0.32	0.11	0.60	0.28

Table 5
Mean, standard deviation, maximum, and minimum values of the tropospheric column density of formaldehyde (HCHO) calculated during February 2019 and February 2020 over the BTH, Wuhan, SMA, and TMA regions. All units for the mean, max, and min values are in molecules/cm^2.

	BTH		Wuhan		Seoul		Tokyo	
	2019	2020	2019	2020	2019	2020	2019	2020
Mean	7.4E+15	6.5E+15	7.3E+15	6.5E+15	5.8E+15	4.5E+15	3.9E+15	3.5E+15
Std. deviation	3.7E+15	2.4E+15	3.7E+15	1.5E+15	1.3E+15	1.4E+15	1.2E+15	9.7E+14
Max value	2E+16	1.4E+16	2.6E+16	1.2E+16	1E+16	8.5E+15	7.9E+15	7.1E+15
Min value	−4.3E+15	−6.5E+15	−1.1E+16	1.3E+14	2.6E+15	−2.1E+14	−3.7E+14	−5.2E+13
Percent change	−13.04		−10.38		−22.09		−8.42	

elevation in temperature can increase biogenic emissions of formaldehyde, but less human activity reduces emissions of anthropogenic formaldehyde. However, to reach a more valid conclusion regarding the impact of meteorological factors on formaldehyde, one should analyze the relationship between daily formaldehyde levels and daily meteorological factors in greater detail. Different studies also reported a decrease in VOC concentrations due to the COVID-19 outbreak and its resulting lockdown situations. For example, Li et al. (2020) investigated changes in pollutant levels in the atmosphere of the Yangtze River Delta in China. They found a 37–57% decrease in VOC concentrations in level 1 (24 January to 25 February 2020) and level 2 (26 February to 31 March 2020) response periods, respectively, compared to 2019.

3.4. Sulfur dioxide (SO_2)

Major sources of SO_2 emissions are coal-fired power plants, industrial sections, automobile tailpipes, and volcanoes (Hand et al., 2012; Mishra et al., 2016; Speight, 2017; Wei et al., 2014). Table 6 shows that Wuhan is the only region (of the four main study regions) that experienced significant reductions (almost 71%) in the column density of SO_2 from the previous year while both the SMA and the TMA showed an increase in SO_2 levels. Moreover, the column density of SO_2 over BTH remained unchanged in 2020. As mentioned before, BTH is one of the most industrialized regions in China. As Fig. S5 shows, BTH has 27 coal-fired power plants while Wuhan has only three. Although the COVID-19 outbreak and the following lockdown

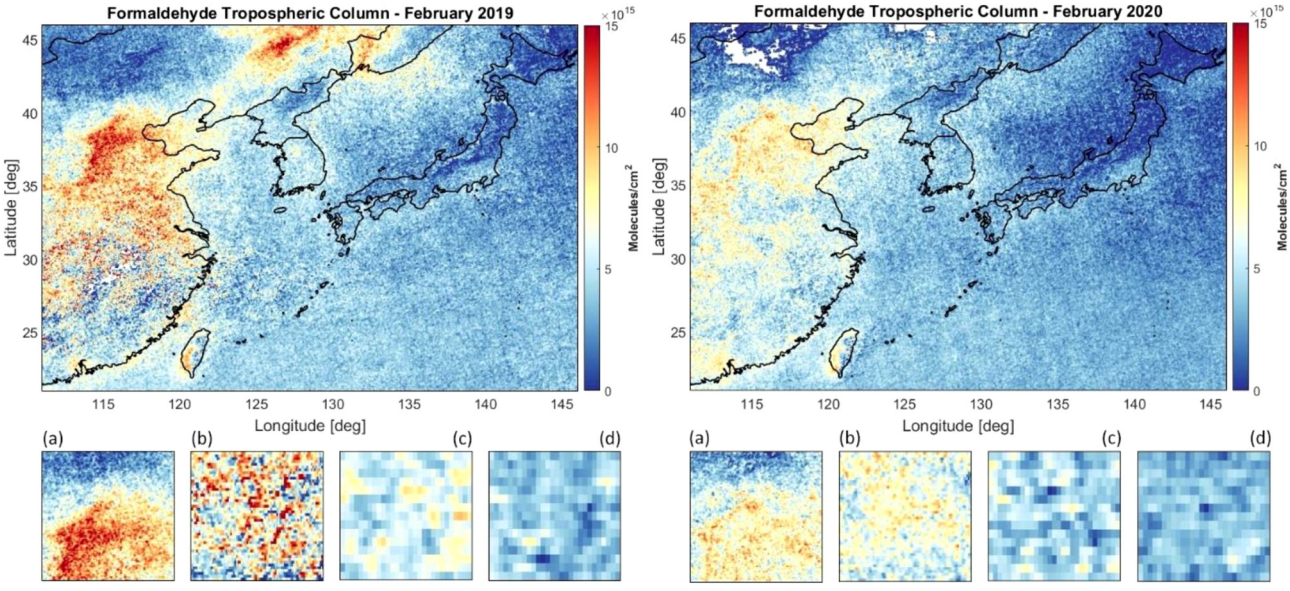

Fig. 5. Map of East Asia showing the tropospheric column density of formaldehyde (HCHO) averaged in February 2019 and February 2020 over the study area. (a), (b), (c), and (d) refer to the BTH, Wuhan, SMA, and TMA regions, respectively. All units for the tropospheric column density of formaldehyde (HCHO) are in molecules/cm^2.

Table 6
Mean, standard deviation, maximum, and minimum values of the total column density of sulfur dioxide (SO_2) calculated in February 2019 and February 2020 over the BTH, Wuhan, SMA, and TMA regions. All units for mean, max, and min values are in molecules/cm^2.

	BTH		Wuhan		Seoul		Tokyo	
	2019	2020	2019	2020	2019	2020	2019	2020
Mean	1.3E+16	1.3E+16	3.9E+15	1.1E+15	8.2E+15	1.1E+16	2.7E+15	9.4E+15
Std. deviation	1.4E+16	1.1E+16	2.3E+16	8.1E+15	9.8E+15	8.4E+15	8.1E+15	8E+15
Max value	8.1E+16	7.3E+16	1.2E+17	4.2E+16	4.3E+16	4.2E+16	2.5E+16	3.4E+16
Min value	−5.4E+16	−4.4E+16	−1.3E+17	−2.8E+16	−2.6E+16	−1.6E+16	−2.2E+16	−1.2E+16
Percent change	−0.01		−71.48		+38.14		+243.43	

significantly decreased SO_2 emissions from vehicle exhaust, the high number of coal-fired power plants and industrial sections in BTH could explain why SO_2 levels remained unchanged. It is also worth mentioning that because of the lockdown and stay-at-home advisory, residents remained in their homes, which increased electricity usage during cold days. The increased demand forced power plants to produce more electricity, resulting in higher emissions of SO_2. Unlike in BTH, in Wuhan, several industrial sections either shut down or worked with limited capacity (Esfandiari and Morris, 2020; Kawakami and Tabeta, 2020). Since Wuhan is home to only three power plants, industry rather than coal-fired power plants is the main source of SO_2 emissions in Wuhan (Li et al., 2017; Qian et al., 2016). Thus, we attribute the significant reductions in SO_2 levels in Wuhan to the shutdown of the industrial sections and the stoppage of full-scale production of many industries (Esfandiari and Morris, 2020; Kawakami and Tabeta, 2020), the main sources of SO_2 emissions in Wuhan. In addition, fewer vehicle emissions also partially decreased levels of SO_2 in Wuhan. Fig. 6 shows the distribution of the total column density of SO_2 over the study area in February 2019 and February 2020. Previous studies also reported significant reductions of SO_2 concentrations due to the lockdown down situations. Otmani et al. (2020) reported a 49% decrease of SO_2 levels in Salé, Morocco, during the COVID-19 lockdown period, compared to the days before the lockdown. Kanniah et al. (2020) also found a 9–20% decrease in SO_2 levels in urban regions of Malaysia during the lockdown situations, compared to the same periods in 2018 and 2019.

As mentioned before, the total column density of SO_2 in the SMA and the TMA was 38 and 243% higher in 2020 than it was in 2019. Figs. S6 and S7 show few coal-fired power plants in these areas, indicating other possible reasons for their dramatic increase in SO_2 levels. Fig. S3 displays the wind patterns in the study area and upwind regions of the SMA and the TMA. The wind patterns, displayed in Fig. 6, reveal that upwind regions of these areas in 2020 were much more polluted than they were in 2019. Considering the velocity of wind emanating from upwind regions (Fig. S3) and the one to three days lifetime of SO_2 in the atmosphere (Lee et al., 2011; Rotstayn and Lohmann, 2002), along with the close proximity of their upwind regions, we conclude that SO_2 was transported from the polluted upwind regions, resulting in a dramatic increase in SO_2 levels in these two areas. Furthermore, Fig. S3 displays only surface wind speeds; wind speeds at higher altitudes, however, are expected to be much higher. Thus, owing to the relatively high frequency of missing values in the daily measurements of the total column density of SO_2 within the four regions, we did not analyze the daily trends of SO_2. Table S4 displays the correlation between each pixel showing the changes in SO_2 concentrations from 2019 to 2020 and its corresponding pixels showing changes in the meteorological patterns from 2019 to 2020 over the four regions. It also shows that meteorological factors are not the determining factors of changes in the SO_2 levels in each region. To reach a more valid conclusion, one should investigate the relationships between daily SO_2 levels and daily meteorological factors in a detailed analysis. Moreover, standard deviation of SO_2 concentrations in Wuhan decreased dramatically in 2020, compared to 2019, indicating a more homogeneous levels of SO_2 in all areas within the Wuhan region in 2020.

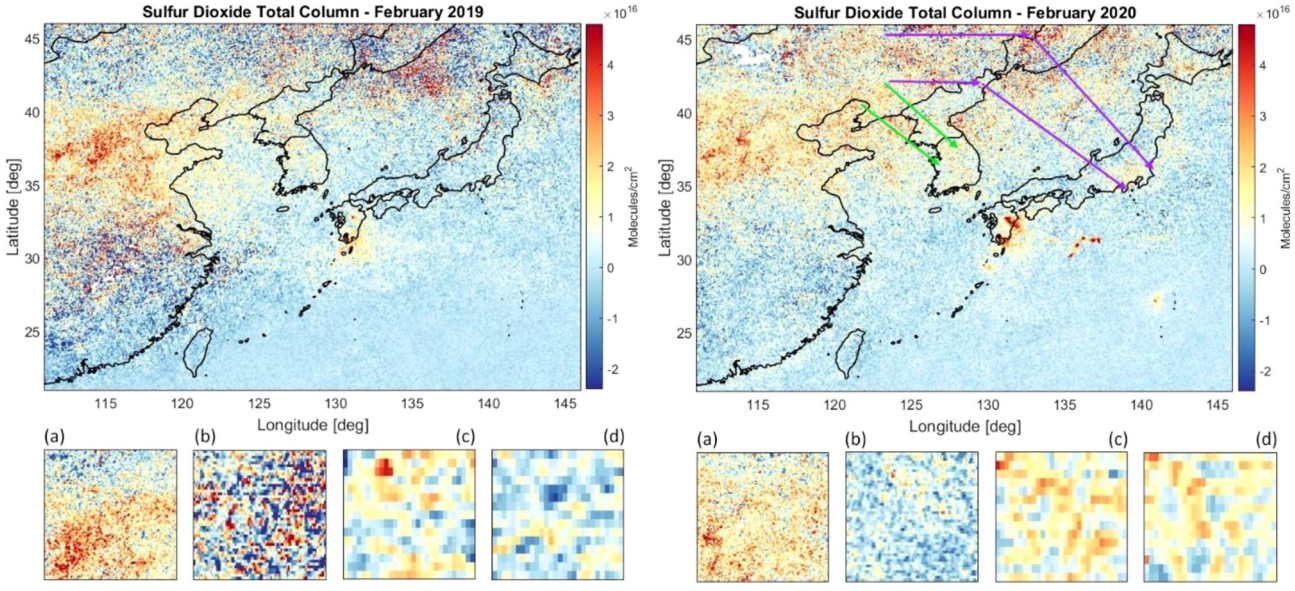

Fig. 6. Map of East Asia showing the total column density of sulfur dioxide (SO_2) averaged in February 2019 and February 2020 over the study area. (a), (b), (c), and (d) refer to the BTH, Wuhan, SMA, and TMA regions, respectively. All units for the total column density of sulfur dioxide (SO_2) are in molecules/cm^2. The purple and green arrows show the wind direction from upwind regions of the TMA and the SMA, respectively.

Table 7
Mean, standard deviation, maximum, and minimum values of the total column density of carbon monoxide (CO) calculated during February 2019 and February 2020 over the BTH, Wuhan, SMA, and TMA. All units for mean, max, and min values are in molecules/cm^2.

	BTH		Wuhan		SMA		TMA	
	2019	2020	2019	2020	2019	2020	2019	2020
Mean	3.23E+18	2.98E+18	3.51E+18	3.38E+18	2.95E+18	2.77E+18	2.51E+18	2.48E+18
Std. deviation	8.10E+17	6.43E+17	3.74E+17	1.87E+17	9.14E+16	9.09E+16	7.54E+16	5.35E+16
Max value	6.36E+18	5.46E+18	4.84E+18	3.99E+18	3.19E+18	2.99E+18	2.71E+18	2.69E+18
Min value	1.78E+18	1.68E+18	2.24E+18	2.77E+18	2.68E+18	2.54E+18	2.27E+18	2.34E+18
Percent change	−7.76		−3.75		−6.41		−1.15	

3.5. Carbon monoxide (CO)

As a major source of CO in the atmosphere is incomplete combustion by automobiles, trucks, and airplanes. Other important sources are wood and grass burning (Choi et al., 2010; Jacobson, 2005). Similar to the total column density of the three pollutants and the AOD, CO also decreased by about 8% in BTH, 4% in Wuhan, 6% in the SMA, and 1% in the TMA (see Table 7). Fig. 7 shows the distribution of the column density of CO over the study area in February 2019 and February 2020. One explanation for the smaller decrease in CO concentrations is that like HCHO, anthropogenic CO emissions resulting from less human activity declined; however, biogenic isoprene emission increased because of the increases in temperature, particularly in Wuhan. The rise in temperature resulted in the oxidation of more biogenic VOC emissions, which increased concentrations of HCHO and CO. Another is that CO has a moderate lifetime of almost two months in the atmosphere (Choi et al., 2010; Lelieveld et al., 2002; Pouyaei et al., 2020). Although emissions of CO decreased significantly, it would take about two months for CO concentrations in the atmosphere to begin to decrease. Table S4 displays the relationship between each pixel showing changes in CO concentrations from 2019 to 2020 and its corresponding pixel showing changes in the meteorological patterns from 2019 to 2020 over the four regions. Although the low correlations indicate a weak relationship between CO levels and meteorological factors, validating this argument would require a more detailed analysis of the relationship between daily CO levels and daily meteorological factors. Because of the relatively high frequency of missing values in the daily measurements of the total column density of CO within the four regions, we did not analyze the daily trends of CO. Moreover, Table 7 shows that the standard deviation of the CO concentrations decreased in all the four regions of the study area, particularly in Wuhan in 2020, compared to 2019. This indicates that CO concentrations are more equally distributed in all the four regions, especially in Wuhan in 2020, compared to 2019. Previous studies also showed decrease in CO levels during the lockdown situations. As an example, Kanniah et al. (2020) reported 25–31% decrease in CO concentrations in urban regions of Malaysia during the lockdown situations, compared to the same periods in 2018 and 2019. They also found notable reductions of CO concentrations in industrial, suburban, and rural regions of Malaysia.

3.6. Formaldehyde to nitrogen dioxide ratio (FNR) and chemical regimes

TROPOMI data showed that the decrease in nitrogen dioxide (NO_2) and formaldehyde (HCHO) concentrations during the lockdown period significantly influenced the sensitivity of ozone formation to ozone precursors, nitrogen oxides ($NO_x = NO + NO_2$), and volatile organic compounds (VOCs). Several studies (Duncan et al., 2010; Haagen-Smit, 1952) have found that in the presence of sunlight, NO_x, and VOCs are the pollutants most responsible for the formation of high ozone concentrations. The photochemical oxidation of VOCs leads to the production of hydroperoxyl (HO_2) and organic peroxy radicals (RO_2), which in turn increase the rate of the catalytic cycling of NO to NO_2 and the formation of high concentrations of ozone at ground level. The cycle is terminated by the oxidation of NO_2 to nitric acid (HNO_3) and the conversion of RO_2 to peroxides (Witte et al., 2011). Ozone production efficiency (OPE) can be defined as the total number of ozone molecules produced when a molecule of NO_x is oxidized and

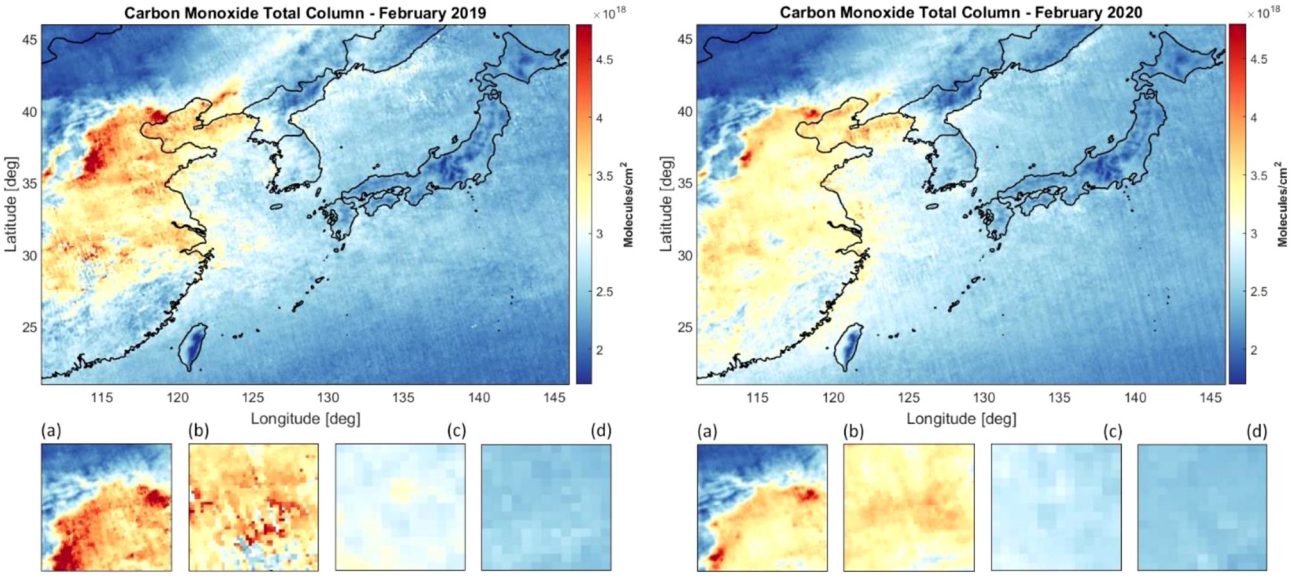

Fig. 7. Map of East Asia showing the total column density of carbon monoxide (CO) averaged in February 2019 and February 2020 over the study area. (a), (b), (c), and (d) refer to the BTH, Wuhan, SMA, and TMA regions, respectively. All units for the total column density of carbon monoxide (CO) are in molecules/cm^2.

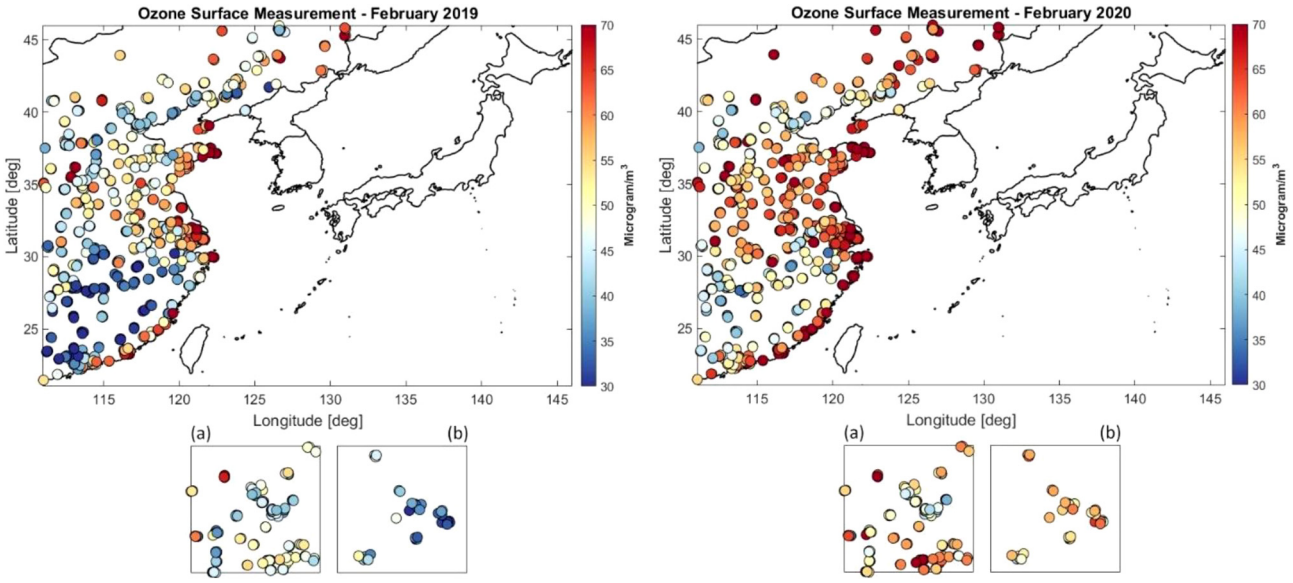

Fig. 8. Map of East Asia showing the ozone surface measurements for February 2019 and February 2020 over the study area. (a) and (b) refer to the BTH and Wuhan regions, respectively. All units for ozone surface measurements are in microgram/m^3.

has a nonlinear relationship with concentrations of its precursors so that ozone concentrations depend on both the absolute and relative concentrations of NO_x and VOCs (Duncan and Chameides, 1998; Jeon et al., 2014).

Several studies (Choi et al., 2012; Duncan et al., 2010; Witte et al., 2011) used the FNR to determine the chemical sensitivity of ozone production (OP) by using models such as the Community Multiscale Air Quality (CMAQ) model. They found that FNR < 1, an FNR between 1 and 2, and FNR > 2 can refer to VOC-sensitive, mixed, and NO_x-sensitive regimes, respectively. The reason for selecting these thresholds is that in VOC-sensitive conditions, an increase (or a decrease) in VOC (NO_x) leads to an increase in ozone concentrations; in NO_x-sensitive conditions, however, ozone increases as NO_x levels increase. Moreover, an FNR between 1 and 2 (mixed regime) reflects the transition between regimes, in which both NO_x and VOCs can change the OP. In this study, we also used the FNR to investigate the chemical sensitivity of the OP to its precursors even though it was not feasible to use satellite images to determine the specific boundaries of the FNR describing VOC-sensitive, mixed, and NO_x-sensitive regimes. Moreover, when the column density of NO_2 is $<1 \times 10^{15}$ molecules cm^{-2}, typical of regions remote to anthropogenic sources, calculating the FNR is not feasible (e.g., Choi et al., 2012; Martin et al., 2006; Russell et al., 2010). As shown in Table S5 and Fig. S8, The FNR significantly increased in the BTH (75%) and Wuhan (398%) regions between 2019 and 2020. Despite increasing dramatically in BTH and Wuhan, the FNR did not do so in either the SMA (16%) or the TMA (20%). East China, especially Wuhan and BTH, imposed more stringent lockdown situations, reducing NO_x and VOC emissions. As described in Sections 3.2 and 3.3, the NO_2 levels decreased by 83% in Wuhan and 54% in BTH in 2020; formaldehyde levels, however, decreased by only 10% in Wuhan and 13% in BTH. This finding indicates that NO_2 was the main factor responsible for the change in the chemical regimes in the BTH and Wuhan regions.

Fig. S9 shows that values of the FNR in most parts of East China, especially in Wuhan, changed from below 1 to above 2, indicating that ozone production in most of these regions became less NO_x saturated in February 2020. Interestingly, ground measurements showed that despite the reductions in NO_2 and formaldehyde concentrations in 2020, surface ozone increased in most parts of East China (Fig. 8), suggesting that the reductions in NO_x and formaldehyde in February 2020 were not sufficiently high to decrease ozone concentrations. Studies (Gao et al., 2020; Ma et al., 2020; Zhu et al., 2017) have reported increases in surface ozone concentrations in recent years, underscoring the challenge that China has faced while attempting to reduce surface ozone. Table 8 shows the surface ozone concentrations in East China, BTH, and Wuhan regions for 2019 and 2020 and the relationship between daily ozone and daily meteorological factors. As shown, ground-level ozone concentrations increased by 19.6% in East China, 16.9% in BTH, and 49.8% in Wuhan. These results show that increases in surface ozone in East China, especially in Wuhan, were not associated with changes in meteorological factors but that they were due to other factors.

4. Conclusion

During the COVID-19 outbreak, there was a dramatic decrease in human activities, resulting in significant reductions in pollutant levels in the atmosphere. In this study, we used satellite remote sensing to investigate the impact of the COVID-19 outbreak on atmospheric concentrations of pollutants, including NO_2, formaldehyde, SO_2, and CO. In this regard, we compared levels of pollutants and the AOD in February 2019 and February 2020. Of the four pollutant concentrations, NO_2 concentrations decreased the most from 2019 to 2020: 54% in BTH, 83% in Wuhan, 33% in the SMA, and 19% in the TMA. Results showed a delay in NO_2 reductions in the SMA resulting from the delay in the COVID-19 outbreak and subsequent stay-at-home strategies in the SMA compared to the BTH and Wuhan. As expected, compared to the other three regions, Wuhan experienced the greatest reductions in

Table 8
Monthly mean values for surface ozone concentrations calculated in February 2019 and February 2020 over East China, BTH, and Wuhan regions along with the correlations between daily ozone and daily meteorological factors. The abbreviations Cor., Temp, Press, and Hum refer to correlation, air temperature (k), surface pressure (hPa), and specific humidity (kg/kg), respectively. All units for ozone concentrations are in microgram/m^3.

	East China		BTH		Wuhan	
	2019	2020	2019	2020	2019	2020
O_3 concentrations	48.5	58	47.3	55.3	37.1	55.6
Cor. O_3 & temp	−0.09	−0.03	−0.07	0.08	0.09	0.19
Cor. O_3 & hum	−0.14	−0.16	−0.11	−0.08	−0.12	−0.14
Cor. O_3 & press	−0.03	0.09	−0.15	−0.06	−0.09	0.09
O_3 percent change	+19.6		+16.9		+49.8	

pollutant levels with 83%, 11%, 71%, and 4% decreases in the column density of NO_2, formaldehyde, SO_2, and CO, respectively, in February 2020. The AOD also decreased by about 62% in Wuhan. Although SO_2 decreased dramatically in Wuhan, it remained relatively unchanged in BTH, due to the larger number of power plants and industrial sections, some of the main sources of SO_2 that remained open in BTH. All of the pollutants except for SO_2 in the SMA and the TMA decreased in 2020. The reason for the increase in SO_2 levels of 30% in the SMA and 243% in the TMA was the effects of transport from polluted upwind regions, which were much more polluted in 2020 than in 2019. Transport from upwind regions was also responsible for the 20% increase in AOD levels in the SMA.

Analyses showed that the mean FNR increased dramatically in BTH (75%) and Wuhan (398%) from 2019 to 2020, while the SMA and the TMA did not experience major changes, a moderate 16% increase in the SMA and 20% in the TMA. This increase in the FNR suggests that OP in all four regions, especially in BTH and Wuhan, became more sensitive to NO_x in 2020. We also investigated surface ozone concentrations in eastern China. Despite the reductions in ozone precursors, NO_x, and formaldehyde, the surface ozone levels in 2020 measured increases of nearly 20% in East China, 17% in BTH, and 50% in Wuhan, suggesting that reductions in NO_x and formaldehyde in 2020 were not high enough to decrease ozone concentrations over East Asia. As investigations of meteorological data revealed that meteorological factors were not strongly correlated with the column density of NO_2 and the surface measurements of ozone, they were not the main factors responsible for changes in NO_2 and surface ozone levels. In addition, we assume that PM levels also decreased from 2019 to 2020 because of reductions in the atmospheric precursors of PM, including SO_2, VOCs, and NO_x.

CRediT authorship contribution statement

Masoud Ghahremanloo: Data curation, Formal analysis, Methodology, Project administration, Software, Validation, Visualization, Writing - original draft, Writing - review & editing. **Yannic Lops:** Data curation, Visualization, Writing - original draft, Writing - review & editing. **Yunsoo Choi:** Conceptualization, Funding acquisition, Methodology, Supervision, Writing - original draft, Writing - review & editing. **Seyedali Mousavinezhad:** Data curation.

Declaration of competing interest

The authors declare that they have no known competing financial interests or personal relationships that could have appeared to influence the work reported in this paper.

Acknowledgments

This study was supported by the High Priority Area Research Grant of the University of Houston.

Appendix A. Supplementary data

Supplementary data to this article can be found online at https://doi.org/10.1016/j.scitotenv.2020.142226.

References

Ainsworth, E.A., 2017. Understanding and improving global crop response to ozone pollution. Plant J. 90 (5), 886–897.

Baltaci, H., 2017. Spatial and temporal variation of the extreme Saharan dust event over Turkey in March 2016. Atmosphere 8 (2), 41.

Baltaci, H., Alemdar, C.S.O., Akkoyunlu, B.O., 2020. Background atmospheric conditions of high PM_{10} concentrations in Istanbul, Turkey. Atmospheric Pollution Research 11 (9), 1524–1534.

Benaissa, F., Bendahmane, I., Bourfis, N., Aoulaiche, O., Alkama, R., 2019. Bioindication of urban air polycyclic aromatic hydrocarbons using petunia hybrida. Civil Engineering Journal 5 (10.28991).

Bessho, K., Date, K., Hayashi, M., Ikeda, A., Imai, T., Inoue, H., ... Okuyama, A., 2016. An introduction to Himawari-8/9—Japan's new-generation geostationary meteorological satellites. Journal of the Meteorological Society of Japan. Ser. II 94 (2), 151–183.

Brunekreef, B., Holgate, S.T., 2002. Air pollution and health. Lancet 360 (9341), 1233–1242.

Chen, L.W.A., Doddridge, B.G., Dickerson, R.R., Chow, J.C., Mueller, P.K., Quinn, J., Butler, W.A., 2001. Seasonal variations in elemental carbon aerosol, carbon monoxide and sulfur dioxide: implications for sources. Geophys. Res. Lett. 28 (9), 1711–1714.

Chen, R., Li, Y., Ma, Y., Pan, G., Zeng, G., Xu, X., ... Kan, H., 2011. Coarse particles and mortality in three Chinese cities: The China Air Pollution and Health Effects Study (CAPES). Science of the total environment 409 (23), 4934–4938.

Chen, R., Kan, H., Chen, B., Huang, W., Bai, Z., Song, G., Pan, G., 2012. Association of particulate air pollution with daily mortality: the China air pollution and health effects study. Am. J. Epidemiol. 175 (11), 1173–1181.

Choi, Y., 2013. The impact of satellite-adjusted NO_x emissions on simulated NO_x and O_3 discrepancies in the urban and outflow areas of the Pacific and Lower Middle US. Atmospheric Chemistry and Physics Discussions 13 (8), 21159–21201.

Choi, Y., Kim, J., Eldering, A., Osterman, G., Yung, Y.L., Gu, Y., Liou, K.N., 2009. Lightning and anthropogenic NO_x sources over the United States and the western North Atlantic Ocean: impact on OLR and radiative effects. Geophys. Res. Lett. 36 (17).

Choi, Y., Osterman, G., Eldering, A., Wang, Y., Edgerton, E., 2010. Understanding the contributions of anthropogenic and biogenic sources to CO enhancements and outflow observed over North America and the western Atlantic Ocean by TES and MOPITT. Atmos. Environ. 44 (16), 2033–2042.

Choi, Y., Kim, H., Tong, D., Lee, P., 2012. Summertime weekly cycles of observed and modeled NO_x and O3 concentrations as a function of satellite-derived ozone production sensitivity and land use types over the Continental United States. Atmos. Chem. Phys. 12 (14), 6291.

Chudnovsky, A.A., Koutrakis, P., Kloog, I., Melly, S., Nordio, F., Lyapustin, A., ... Schwartz, J., 2014. Fine particulate matter predictions using high resolution Aerosol Optical Depth (AOD) retrievals. Atmospheric Environment 89, 189–198.

de Laat, A., Vazquez-Navarro, M., Theys, N., Stammes, P., 2019. Analysis of properties of the 19 February 2018 volcanic eruption of Mount Sinabung in S5P/TROPOMI and Himawari satellite data. Nat. Hazards Earth Syst. Sci. 2019, 1–19.

Duncan, B.N., Chameides, W.L., 1998. Effects of urban emission control strategies on the export of ozone and ozone precursors from the urban atmosphere to the troposphere. Journal of Geophysical Research: Atmospheres 103 (D21), 28159–28179.

Duncan, B.N., Yoshida, Y., Olson, J.R., Sillman, S., Martin, R.V., Lamsal, L., ... Crawford, J.H., 2010. Application of OMI observations to a space-based indicator of NO_x and VOC controls on surface ozone formation. Atmospheric Environment 44 (18), 2213–2223.

Esfandiari, S., Morris, M. (2020, January 27). These are all the companies who have shut down operations in China over the deadly Wuhan coronavirus outbreak. (Retrieved May 5, 2020 from) https://www.businessinsider.com/wuhan-coronavirus-which-companies-shut-down-operations-move-employees-2020-1.

Gao, C., Xiu, A., Zhang, X., Chen, W., Liu, Y., Zhao, H., Zhang, S., 2020. Spatiotemporal characteristics of ozone pollution and policy implications in Northeast China. Atmospheric Pollution Research 11 (2), 357–369. https://doi.org/10.1016/j.apr.2019.11.008.

Ghahremanloo, M., Mobasheri, M.R., Amani, M., 2019. Soil moisture estimation using land surface temperature and soil temperature at 5 cm depth. Int. J. Remote Sens. 40 (1), 104–117.

Guo, H., Wang, T., Simpson, I.J., Blake, D.R., Yu, X.M., Kwok, Y.H., Li, Y.S., 2004. Source contributions to ambient VOCs and CO at a rural site in eastern China. Atmos. Environ. 38 (27), 4551–4560.

Gupta, P., Christopher, S.A., Wang, J., Gehrig, R., Lee, Y.C., Kumar, N., 2006. Satellite remote sensing of particulate matter and air quality assessment over global cities. Atmos. Environ. 40 (30), 5880–5892.

Haagen-Smit, A.J., 1952. Chemistry and physiology of Los Angeles smog. Industrial & Engineering Chemistry 44 (6), 1342–1346.

Hand, J.L., Schichtel, B.A., Malm, W.C., Pitchford, M.L., 2012. Particulate sulfate ion concentration and SO2 emission trends in the United States from the early 1990s through 2010. Atmos. Chem. Phys. 12 (21), 10353–10365.

Hodan, W.M., Barnard, W.R., 2004. Evaluating the Contribution of PM2.5 Precursor Gases and Re-Entrained Road Emissions to Mobile Source PM2. 5 Particulate Matter Emissions. MACTEC Federal Programs, Research Triangle Park, NC.

Hoesly, R.M., Smith, S.J., Feng, L., Klimont, Z., Janssens-Maenhout, G., Pitkanen, T., ... Bond, T.C., 2018. Historical (1750–2014) anthropogenic emissions of reactive gases and aerosols from the Community Emissions Data System (CEDS). Geoscientific Model Development 11 (Online). (PNNL-SA-123932).

Jacobson, M.Z., 2005. Fundamentals of Atmospheric Modeling. Cambridge university press.

Jeon, W.B., Lee, S.H., Lee, H., Park, C., Kim, D.H., Park, S.Y., 2014. A study on high ozone formation mechanism associated with change of NOx/VOCs ratio at a rural area in the Korean Peninsula. Atmos. Environ. 89, 10–21.

Kanniah, K.D., Zaman, N.A.F.K., Kaskaoutis, D.G., Latif, M.T., 2020. COVID-19's impact on the atmospheric environment in the Southeast Asia region. Sci. Total Environ. 139658.

Kawakami, T., Tabeta, S., (2020, February 3). Wuhan lockdown strikes at heart of 'Made in China 2025. Retrieved May 5, 2020, from https://asia.nikkei.com/Spotlight/Coronavirus/Wuhan-lockdown-strikes-at-heart-of-Made-in-China-2025.

Kim, M. J. and Denyer, S. (2020, February 25). In South Korea, a region is stricken with coronavirus. But no China-style lockdown is planned. Retrieved May 5, 2020, from https://www.washingtonpost.com/world/asia_pacific/inSouthKoreaaregionisstrickenwithcoronavirusbutnochina-stylelockdownsplanned/2020/02/25/a0e90bf0-57b8-11ea-8efd-0f904bdd8057_story.html.

Kim, H.C., Kim, E., Bae, C., Cho, J.H., Kim, B.U., Kim, S., 2017. Regional contributions to particulate matter concentration in the Seoul metropolitan area, South Korea: seasonal variation and sensitivity to meteorology and emissions inventory. Atmospheric Chemistry & Physics 17 (17).

Köhler, P., Frankenberg, C., Magney, T.S., Guanter, L., Joiner, J., Landgraf, J., 2018. Global retrievals of solar-induced chlorophyll fluorescence with TROPOMI: first results and intersensor comparison to OCO-2. Geophys. Res. Lett. 45 (19), 10–456.

Kramar, M., Ignatov, A., Petrenko, B., Kihai, Y., Dash, P., 2016, May. Near real time SST retrievals from Himawari-8 at NOAA using ACSPO system. Ocean Sensing and Monitoring VIII. vol. 9827. International Society for Optics and Photonics, p. 98270L.

Lee, C., Martin, R.V., van Donkelaar, A., Lee, H., Dickerson, R.R., Hains, J.C., ... Schwab, J.J., 2011. SO_2 emissions and lifetimes: Estimates from inverse modeling using in situ and global, space-based (SCIAMACHY and OMI) observations. Journal of Geophysical Research: Atmospheres 116 (D6).

Lee, S., Song, C.H., Park, R.S., Park, M.E., Han, K.M., Kim, J., ... Woo, J.H., 2015. Development of a numerical system to improve particulate matter forecasts in South Korea using geostationary satellite-retrieved aerosol optical data over Northeast Asia. Geoscientific Model Development Discussions 8 (11).

Lee, Y., Ahn, M.H., Kang, M., 2020. The new potential of deep convective clouds as a calibration target for a geostationary UV/VIS Hyperspectral spectrometer. Remote Sens. 12 (3), 446.

Lelieveld, J., Peters, W., Dentener, F.J., Krol, M.C., 2002. Stability of tropospheric hydroxyl chemistry. Journal of Geophysical Research: Atmospheres 107 (D23), ACH–17.

Li, M., Zhang, Q., Kurokawa, J.-I., Woo, J.-H., He, K., Lu, Z., Ohara, T., Song, Y., Streets, D.G., Carmichael, G.R., Cheng, Y., Hong, C., Huo, H., Jiang, X., Kang, S., Liu, F., Su, H., Zheng, B., 2017. MIX: a mosaic Asian anthropogenic emission inventory under the international collaboration framework of the MICS-Asia and HTAP. Atmos. Chem. Phys. 17, 935–963. https://doi.org/10.5194/acp-17-935-2017.

Li, J., Liao, H., Hu, J., Li, N., 2019. Severe particulate pollution days in China during 2013–2018 and the associated typical weather patterns in Beijing-Tianjin-Hebei and the Yangtze River Delta regions. Environ. Pollut. 248, 74–81.

Li, L., Li, Q., Huang, L., Wang, Q., Zhu, A., Xu, J., ... Azari, M., 2020. Air quality changes during the COVID-19 lockdown over the Yangtze River Delta Region: An insight into the impact of human activity pattern changes on air pollution variation. Science of The Total Environment 139282.

Liu, H., Liu, S., Xue, B., Lv, Z., Meng, Z., Yang, X., ... He, K., 2018. Ground-level ozone pollution and its health impacts in China. Atmospheric environment 173, 223–230.

Loveland, T.R., Dwyer, J.L., 2012. Landsat: building a strong future. Remote Sens. Environ. 122, 22–29.

Lu, Z., Streets, D.G., Zhang, Q., Wang, S., Carmichael, G.R., Cheng, Y.F., Tan, Q., 2010. Sulfur dioxide emissions in China and sulfur trends in East Asia since 2000. Atmospheric Chemistry & Physics 10 (13).

Luecken, D.J., Hutzell, W.T., Strum, M.L., Pouliot, G.A., 2012. Regional sources of atmospheric formaldehyde and acetaldehyde, and implications for atmospheric modeling. Atmos. Environ. 47, 477–490.

Ma, Y., Ma, B., Jiao, H., Zhang, Y., Xin, J., Yu, Z., 2020. An analysis of the effects of weather and air pollution on tropospheric ozone using a generalized additive model in Western China: Lanzhou, Gansu. Atmos. Environ. 224, 117342. https://doi.org/10.1016/j.atmosenv.2020.117342.

Mao, L., Liu, R., Liao, W., Wang, X., Shao, M., Liu, S.C., Zhang, Y., 2019. An observation-based perspective of winter haze days in four major polluted regions of China. Natl. Sci. Rev. 6 (3), 515–523.

Martin, R.V., 2008. Satellite remote sensing of surface air quality. Atmos. Environ. 42 (34), 7823–7843.

Martin, R.V., Jacob, D.J., Chance, K., Kurosu, T.P., Palmer, P.I., Evans, M.J., 2003. Global inventory of nitrogen oxide emissions constrained by space-based observations of NO_2 columns. Journal of Geophysical Research: Atmospheres 108 (D17).

Martin, R.V., Sioris, C.E., Chance, K., Ryerson, T.B., Bertram, T.H., Wooldridge, P.J., ... Flocke, F.M., 2006. Evaluation of space-based constraints on global nitrogen oxide emissions with regional aircraft measurements over and downwind of eastern North America. Journal of Geophysical Research: Atmospheres 111 (D15).

Masuoka, E., Fleig, A., Wolfe, R.E., Patt, F., 1998. Key characteristics of MODIS data products. IEEE Trans. Geosci. Remote Sens. 36 (4), 1313–1323.

Mehdipour, V., Memarianfard, M., 2017. Application of support vector machine and gene expression programming on tropospheric ozone prognosticating for Tehran metropolitan. Civ Eng J 3 (8), 557–567.

Mhawish, A., Kumar, M., Mishra, A.K., Srivastava, P.K., Banerjee, T., 2018. Remote sensing of aerosols from space: retrieval of properties and applications. Remote Sensing of Aerosols, Clouds, and Precipitation. Elsevier, pp. 45–83.

Mishra, R.K., Shukla, A., Parida, M., Pandey, G., 2016. Urban roadside monitoring and prediction of CO, NO2 and SO2 dispersion from on-road vehicles in megacity Delhi. Transp. Res. Part D: Transp. Environ. 46, 157–165.

Mulenga, D., Siziya, S., 2019. Indoor air pollution related respiratory ill health, a sequel of biomass use. SciMedicine Journal 1 (1), 30–37.

Normile, D., Heidt, May, A., Stokstad, E., Heidt, A., Heidt, A., & Heidt, A. (2020, March 18). Coronavirus cases have dropped sharply in South Korea. What's the secret to its success? Retrieved May 5, 2020, from https://www.sciencemag.org/news/2020/03/coronaviruscaseshavedroppedsharplySouthKoreawhat'ssecretitssuccess. (doi: 10.1126/science. abb7566).

Nuvolone, D., Petri, D., Voller, F., 2018. The effects of ozone on human health. Environ. Sci. Pollut. Res. 25 (9), 8074–8088.

Otmani, A., Benchrif, A., Tahri, M., Bounakhla, M., El Bouch, M., Krombi, M.H., 2020. Impact of Covid-19 lockdown on PM10, SO2 and NO2 concentrations in Salé City (Morocco). Sci. Total Environ. 139541.

Pan, S., Choi, Y., Roy, A., Li, X., Jeon, W., Souri, A.H., 2015. Modeling the uncertainty of several VOC and its impact on simulated VOC and ozone in Houston, Texas. Atmos. Environ. 120, 404–416.

Placet, M., Mann, C.O., Gilbert, R.O., Niefer, M.J., 2000. Emissions of ozone precursors from stationary sources: a critical review. Atmos. Environ. 34 (12–14), 2183–2204.

Pouyaei, A., Choi, Y., Jung, J., Sadeghi, B., Song, C.H., 2020. Concentration trajectory route of air pollution with an integrated Lagrangian model (C-TRAIL model v1.0) derived from the community multiscale air quality Modeling (CMAQ model v5.2). Geoscientific Model Development Discussions 13 (8), 3489–3505. https://doi.org/10.5194/gmd-2019-366.

Qian, Z., Liang, S., Yang, S., Trevathan, E., Huang, Z., Yang, R., ... Shen, L., 2016. Ambient air pollution and preterm birth: a prospective birth cohort study in Wuhan, China. International journal of hygiene and environmental health 219 (2), 195–203.

Reed, C., Evans, M.J., Di Carlo, P., Lee, J.D., Carpenter, L.J., 2016. Interferences in photolytic NO_2 measurements: explanation for an apparent missing oxidant? Atmos. Chem. Phys. 4707–4724.

Richman, D.D., Whitley, R.J., Hayden, F.G., 2016. Clinical Virology. John Wiley & Sons.

Richter, A., Burrows, J.P., Nüß, H., Granier, C., Niemeier, U., 2005. Increase in tropospheric nitrogen dioxide over China observed from space. Nature 437 (7055), 129–132.

Rotstayn, L.D., Lohmann, U., 2002. Simulation of the tropospheric sulfur cycle in a global model with a physically based cloud scheme. Journal of Geophysical Research: Atmospheres 107 (D21) (AAC-20).

Rush, J. (2020, April 12). No lockdown in Japan: request-based emergency measures having limited effect in reducing crowds. Retrieved May 5, 2020, from https://www.forbes.com/sites/joelrush/2020/04/12/nolockdowninjapanrequestbasedemergencymeasureshavinglimitedeffectinreducingcrowds/#16627a2430e9.

Russell, A.R., Valin, L.C., Bucsela, E.J., Wenig, M.O., Cohen, R.C., 2010. Space-based constraints on spatial and temporal patterns of NO_x emissions in California, 2005—2008. Environmental science & technology 44 (9), 3608–3615.

Shim, C., Wang, Y., Choi, Y., Palmer, P.I., Abbot, D.S., Chance, K., 2005. Constraining global isoprene emissions with global ozone monitoring experiment (GOME) formaldehyde column measurements. Journal of Geophysical Research: Atmospheres 110 (D24).

Song, C., Wu, L., Xie, Y., He, J., Chen, X., Wang, T., ... Dai, Q., 2017. Air pollution in China: status and spatiotemporal variations. Environmental pollution 227, 334–347.

Speight, J.G., 2017. Sources and types of inorganic pollutants. Environmental Inorganic Chemistry for Engineers. Butterworth-Heinemann, pp. 231–282.

Trebs, I., Bohn, B., Ammann, C., Rummel, U., Blumthaler, M., Königstedt, R., … & Andreae, M. O. (2009). Relationship between the NO 2 photolysis frequency and the solar global irradiance. Atmospheric Measurement Techniques, 2(2), 725–739.

Van der A, R.J., Mijling, B., Ding, J., Elissavet Koukouli, M., Liu, F., Li, Q., ... Theys, N., 2017. Cleaning up the air: effectiveness of air quality policy for SO_2 and NO_x emissions in China. Atmospheric Chemistry & Physics 17, 1775–1789.

Van Der Werf, G.R., Randerson, J.T., Giglio, L., Collatz, G.J., Kasibhatla, P.S., Arellano Jr., A.F., 2006. Interannual Variability of Global Biomass Burning Emissions From 1997 to 2004.

Veefkind, J.P., Aben, I., McMullan, K., Förster, H., De Vries, J., Otter, G., ... Van Weele, M., 2012. TROPOMI on the ESA Sentinel-5 Precursor: A GMES mission for global observations of the atmospheric composition for climate, air quality and ozone layer applications. Remote Sensing of Environment 120, 70–83.

Viguier, L., 1999. Emissions of SO_2, NO_x and CO_2 in transition economies: emission inventories and Divisia index analysis. Energy J. 20 (2).

Wang, P., Chen, K., Zhu, S., Wang, P., Zhang, H., 2020. Severe air pollution events not avoided by reduced anthropogenic activities during COVID-19 outbreak. Resour. Conserv. Recycl. 158, 104814.

Wei, J., Guo, X., Marinova, D., Fan, J., 2014. Industrial SO_2 pollution and agricultural losses in China: evidence from heavy air polluters. J. Clean. Prod. 64, 404–413.

WHO Timeline - COVID-19. (2020, April 8). Retrieved May 5, 2020, from https://www.who.int/news-room/detail/08-04-2020-who-timeline—covid-19.

Witte, J.C., Duncan, B.N., Douglass, A.R., Kurosu, T.P., Chance, K., Retscher, C., 2011. The unique OMI $HCHO/NO_2$ feature during the 2008 Beijing Olympics: implications for ozone production sensitivity. Atmos. Environ. 45 (18), 3103–3111.

Wu, Y., Zhang, S., Hao, J., Liu, H., Wu, X., Hu, J., ... Stevanovic, S., 2017. On-road vehicle emissions and their control in China: A review and outlook. Science of the Total Environment 574, 332–349.

Wu, Y., Arapi, A., Huang, J., Gross, B., Moshary, F., 2018. Intra-continental wildfire smoke transport and impact on local air quality observed by ground-based and satellite remote sensing in New York City. Atmos. Environ. 187, 266–281.

Yang, Y., Liao, H., Lou, S., 2016. Increase in winter haze over eastern China in recent decades: roles of variations in meteorological parameters and anthropogenic emissions. Journal of Geophysical Research: Atmospheres 121 (21), 13–050.

Yang, Q., Yuan, Q., Li, T., Shen, H., Zhang, L., 2017. The relationships between $PM_{2.5}$ and meteorological factors in China: seasonal and regional variations. Int. J. Environ. Res. Public Health 14 (12), 1510.

Yienger, J.J., Levy, H., 1995. Empirical model of global soil-biogenic NO_x emissions. Journal of Geophysical Research: Atmospheres 100 (D6), 11447–11464.

Yu, Y., Kalashnikova, O.V., Garay, M.J., Notaro, M., 2019. Climatology of Asian dust activation and transport potential based on MISR satellite observations and trajectory analysis. Atmospheric Chemistry & Physics 19 (1).

Zambrano-Monserrate, M.A., Ruano, M.A., Sanchez-Alcalde, L., 2020. Indirect effects of COVID-19 on the environment. Sci. Total Environ. 138813.

Zhang, Q., Geng, G., Wang, S., Richter, A., He, K., 2012. Satellite remote sensing of changes in NO_x emissions over China during 1996–2010. Chin. Sci. Bull. 57 (22), 2857–2864.

Zhang, J., Zhang, L.Y., Du, M., Zhang, W., Huang, X., Zhang, Y.Q., ... Li, Y.W., 2016. Indentifying the major air pollutants base on factor and cluster analysis, a case study in 74 Chinese cities. Atmospheric Environment 144, 37–46.

Zhang, Z., Wang, W., Cheng, M., Liu, S., Xu, J., He, Y., Meng, F., 2017. The contribution of residential coal combustion to $PM_{2.5}$ pollutions over China's Beijing-Tianjin-Hebei region in winter. Atmos. Environ. 159, 147–161.

Zhang, Z., Wu, W., Fan, M., Tao, M., Wei, J., Jin, J., ... Wang, Q., 2019. Validation of Himawari-8 aerosol optical depth retrievals over China. Atmospheric environment 199, 32–44.

Zhao, N., Yue, T., Li, H., Zhang, L., Yin, X., Liu, Y., 2018. Spatio-temporal changes in precipitation over Beijing-Tianjin-Hebei region, China. Atmos. Res. 202, 156–168.

Zheng, B., Tong, D., Li, M., Liu, F., Hong, C., Geng, G., ... Yan, L., 2018. Trends in China's anthropogenic emissions since 2010 as the consequence of clean air actions. Atmospheric Chemistry and Physics 18 (19), 14095–14111.

Zhu, J., Liao, H., Mao, Y., Yang, Y., Jiang, H., 2017. Interannual variation, decadal trend, and future change in ozone outflow from East Asia. In. Atmos. Chem. Phys. 17 (5), 3729–3747 Copernicus GmbH. https://doi.org/10.5194/acp-17-3729-2017.